

Bright gamma-ray Galactic Center excess and dark dwarfs: Strong tension for dark matter annihilation despite Milky Way halo profile

Kevork N. Abazajian* and Ryan E. Keeley†
*Center for Cosmology, Department of Physics and Astronomy,
 University of California, Irvine, Irvine, California 92697 USA*

We incorporate Milky Way dark matter halo profile uncertainties, as well as an accounting of diffuse gamma-ray emission uncertainties in dark matter annihilation models for the Galactic Center Extended gamma-ray excess (GCE) detected by the Fermi Gamma Ray Space Telescope. The range of particle annihilation rate and masses expand when including these unknowns. However, two of the most precise empirical determinations of the Milky Way halo’s local density and density profile leave the signal region to be in considerable tension with dark matter annihilation searches from combined dwarf galaxy analyses for single-channel dark matter annihilation models. The GCE and dwarf tension can be alleviated if: one, the halo is very highly concentrated or strongly contracted; two, the dark matter annihilation signal differentiates between dwarfs and the GC; or, three, local stellar density measures are found to be significantly lower, like that from recent stellar counts, increasing the local dark matter density.

PACS numbers: 95.35.+d,95.55.Ka,95.85.Pw,97.60.Gb

I. INTRODUCTION

The Milky Way’s Galactic Center (GC) is an exceedingly crowded region with numerous gamma-ray point sources and several sources of diffuse emission. It is also expected to contain a high density of dark matter, which makes it a promising place to search for signals of dark matter annihilation or decay. Weakly Interacting Massive Particles (WIMPs) are among the leading candidates for dark matter, due to a natural mechanism for their thermal production at the proper density in the early Universe. Supersymmetric extensions to the standard model of particle physics can easily accommodate a WIMP [1].

In previous work, several known sources of gamma-ray emission toward the GC have been detected and modeled. There are 18 gamma-ray sources within the $7^\circ \times 7^\circ$ region about the GC within the Second Fermi Gamma-ray LAT Source Catalog (2FGL). For example, the gamma-ray point source associated with Sgr A* is one of the brightest sources in the region and its emission in this band can be modeled as originating from hadronic cosmic rays transitioning from diffuse to rectilinear propagation [2]. There is an abundance of gamma rays associated with bremsstrahlung emission from e^\pm , as mapped by the 20 cm radio map of the GC [3]. There is also Inverse Compton (IC) emission that is consistent with coming from the same e^\pm source as the bremsstrahlung emission [4].

After considering known sources of gamma-ray emission, there remains an extended excess [5–13]. This Galactic Center Extended (GCE) excess signal gained significant interest since it may be consistent with a

WIMP dark matter annihilation model. Primarily, the spatial profile of the excess is consistent with the expected profile from dark matter halos in galaxy formation simulations. Secondly, the strength of the signal implies an interaction cross section that is consistent with the thermal relic cross section. And thirdly, the spectra of the excess signal is consistent with a WIMP with a mass between 10-50 GeV that decays through quark or lepton channels. This triple consistency of the WIMP paradigm as an explanation of the GCE has gained significant attention.

Of course, there exist other candidates for the GCE gamma-ray emission. For instance, there is a large population of compact objects which can be bright gamma-ray sources. The GC Central Stellar Cluster can harbor a significant population of millisecond pulsars (MSPs). Since MSPs can have a spectra similar to low-particle-mass annihilating WIMPs, their presence can confuse a dark matter interpretation of the GC emission [14, 15]. Significantly, flux probability distribution methods have found evidence that point sources are more consistent with the GCE flux map than a smooth halo source [16, 17].

If annihilating dark matter explains the GCE, then there should be annihilation signals in other places that have a high density of dark matter. Two such places are the “inner Galaxy” (within $\sim 20^\circ$ of the GC) and the dwarf satellites of the Milky Way. Previous work has found that the inner galaxy signal is consistent with the mass and cross section supported by the galactic center [12, 13]. We will show the Milky Way dwarf galaxies’ lack of a signal [18, 19] significantly constrains the GCE parameter space. However, there is a reported excess from the newly discovered Reticulum 2 dwarf galaxy that may be consistent with the GC annihilation signal [20]. We will discuss below what would be required to have the GCE signal be consistent with the dwarf galaxy limits.

Previous analyses have largely used fixed values for the parameters of the Milky Way’s dark matter halo when

* keverk@uci.edu

† rkeeley@uci.edu

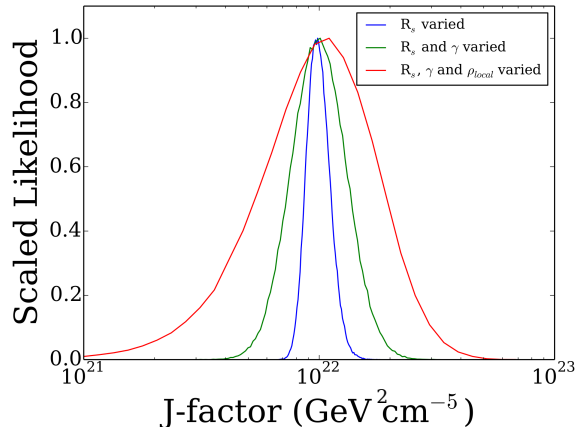


FIG. 1. Plotted is the scaled likelihood for the galactic center’s J-factor for our ROI given relaxation of the constraints on the Milky Way dark matter halo, as described in the text.

inferring dark matter particle properties that could produce the GCE. There exists significant uncertainty in these parameters, which translates into large errors on the cross section of dark matter annihilation, while background emission modeling uncertainties in the crowded GC region largely generate uncertainties on the dark matter particle mass. In this paper, we perform a Bayesian analysis of the full GCE likelihood in order to more properly quantify the uncertainties on the nature of dark matter that may produce the GCE signal. Gaussian and chi-squared statistics are often used in other work for dark matter fits to the GCE spectra. Such approximations are inaccurate due to the Poisson nature of the photon count signal, and the inaccuracy is increased when convolved with Milky Way halo uncertainties. To assist in particle model fits to the GCE, we also provide the tools necessary to accurately calculate these uncertainties for general dark matter annihilation models with arbitrary spectra.¹

II. DATA AND MODEL COMPONENTS

The data set that we will refer to as the ‘IC’ data set is taken from the analysis in Ref. [4]. It is generated with Fermi Tools version `v9r33` to study Fermi LAT observations from August 2008 to June 2014 (approximately 70 months of data). This data is from Pass 7 rather than Pass 7 Reprocessed instrument response functions since the diffuse map associated with the latter have strong caveats for use with new extended sources. This analysis simultaneously fits the amplitude and spectrum of point sources from the 2FGL catalog [21], plus four other

point sources in the region of interest (ROI). It uses 0.2 – 100 GeV photons in 30 logarithmically-spaced energy bins, with ULTRACLEAN-class photon selection. The IC data-set includes the 20 cm radio template as a tracer of gas to account for the bremsstrahlung emission as has been done previously [3, 11, 22]. It also includes IC emission from starlight with a 3.4 μm template from the WISE mission [23]. The IC data set also includes the New Diffuse (ND) map whose intensity is sub-dominant to the bremsstrahlung map and increases with angle away from the GC. The ND template is that described in Ref. [22], and is interpreted as accounting for additional bremsstrahlung emission not captured in the 20 cm map. The IC data set optimized the morphology of the GCE excess and ND templates to their best-fit profiles. The GCE excess, used templates of density $\rho(r)^2$ projected along the line-of-sight with $\rho(r) \propto r^{-\gamma}(r + r_s)^{-(3-\gamma)}$. The IC data analysis found that $\gamma = 1$ provided the best fit. In this IC data set, all the 4 extended sources (GCE, ND, IC, Bremsstrahlung) were given generic log-parabola spectral forms with four free parameters each. The analysis detected the WISE 3.4 μm template at very high significance of $\text{TS} = 197.0^2$. The previously studied sources were also detected at high significance. The GCE was detected with $\text{TS} = 207.5$, bremsstrahlung was detected with $\text{TS} = 97.2$.

We adopt ‘noIC’ and ‘noB’ data sets from the analysis in Ref. [22]. These data sets were analyzed in a similar manner to the ‘IC’ data, except the ‘noIC’ data set does not include the inverse Compton background template, and the ‘noB’ includes neither the inverse Compton template nor the 20 cm radio template. Both these data sets cover the same $7^\circ \times 7^\circ$ ROI as the ‘IC’ set, but use SOURCE-class photons. They use Fermi Tools version `v9r31p1` to study Fermi LAT data from August 2008 to May 2013 (approximately 57 months of data), and they use Pass 7 instrument response functions.

III. ANALYSIS

The signal strength of annihilating dark matter in the GC depends on the density profile of the Milky Way’s dark matter profile. We choose dark matter density to have the generalized Navarro-Frenk-White (NFW) profile of the form [24, 25]:

$$\rho(r) = \frac{\rho_\odot}{\left(\frac{r}{R_\odot}\right)^\gamma \left(\frac{1+r/R_s}{1+R_\odot/R_s}\right)^{3-\gamma}}, \quad (3.1)$$

where R_\odot is the Sun’s distance from the center of the Milky Way, ρ_\odot is the density of the dark matter halo at

¹ https://github.com/rekeeleley/GCE_errors

² $\text{TS} \equiv 2\Delta \ln \mathcal{L}$, where $\Delta \mathcal{L}$ is the difference of the best-fit likelihood with and without the source. For point sources, a value of $\text{TS} = 25$ is detected at a significance of just over 4σ [21].

R_\odot , R_s is the scale radius of the Milky Way’s dark matter halo, and γ is a parameter characterizing the slope of the inner part of the profile.

To arrive at substantially more accurate errors on the inferred dark matter particle mass and cross section from the GCE signal, we employ a Bayesian analysis to propagate uncertainties in the dark matter halo to uncertainties in the particle annihilation parameters. Bayesian techniques have a formally straightforward method to include the effect of these nuisance parameters, namely to integrate the likelihood over the subspace of those nuisance parameters:

$$\mathcal{L}(\theta|x) = \int dn \mathcal{L}(\theta, n|x). \quad (3.2)$$

This defines our approach for this analysis: calculate the full likelihood then marginalize over the nuisance subspace to get the likelihood as a function of the dark matter mass and cross section. The posterior distribution errors are determined and displayed via contours of $\Delta\mathcal{L}$ that enclose the relevant credible interval. Note that our choice of integrand limits in marginalization and parameter priors are always well outside the credible intervals of the parameters of interest. The prior distribution is either flat in logarithmic space, for the concentration (scale radius) log-normal distribution, or flat in the parameter value as the remaining distributions are nearly Gaussian for the parameter values. As we shall show below, our marginalization integral approximations leave our results to be equivalent to the handling of nuisance parameters in frequentist statistics.

The random observable that is used in our Bayesian analysis is the gamma-ray number counts binned by energy. Such number counts have Poisson statistical errors. Hence, to do the Bayesian analysis, it is appropriate to use a log-likelihood of the form:

$$\log(\mathcal{L}) = \sum_i k_i \log \mu_i - \mu_i, \quad (3.3)$$

up to factors that do not involve the model parameters. Here, k_i is the observed number of events in the i -th energy bin and μ_i is the expected number of events from the model in that energy bin. The expected number count in bin i has two components, one associated with the dark matter annihilation, and one associated with background sources. The dark matter number count is given by the integral of the spectra of the number flux over the energy bin, multiplied by the exposure of the i -th bin:

$$\mu_i = b_i + \epsilon_i \int_{E_i}^{E_{i+1}} \frac{d\Phi}{dE} dE, \quad (3.4)$$

where b is the modeled background counts, ϵ is the exposure, $d\Phi/dE$ is the differential number flux, and the integral is over the energy bin from the observed number counts. The differential flux is given by:

$$\frac{d\Phi}{dE} = J \frac{\langle\sigma v\rangle}{8\pi m_\chi^2} \frac{dN}{dE}. \quad (3.5)$$

Here, $\langle\sigma v\rangle$ is the cross-section, m_χ is the mass of the dark matter particle, dN/dE is the per annihilation spectra, and the J-factor is the integral of the square of the dark matter density along the line of sight

$$J(\theta, \phi) = \int dz \rho^2(r(\theta, \phi, z)). \quad (3.6)$$

We use the package PPPC4DMID to generate the prompt annihilation spectra dN/dE [26].

The largest uncertainties on dark matter particle parameters arise from Milky Way halo parameters. It is the Milky Way halo parameters, ρ_\odot , γ , and R_s , that need to be marginalized over. The Milky Way halo parameters are determined either from direct observational constraints, such as that for ρ_\odot and γ , or from that expected for dark matter halos in simulations, for R_s , since no significant observational constraint exists on this scale. The dependence on R_s and its uncertainty, as we shall show, is not significant.

One robust determination of the local dark matter density is derived from modeling the spatial and velocity distributions for a sample of 9000 K-dwarf stars from the Sloan Digital Sky Survey (SDSS) by Zhang et al. [27]. The velocity distribution of these stars directly measures the local gravitational potential and, when combined with stellar density constraints, provides a measure of the local dark matter density. The inferred value for the local dark matter density from that work is $\rho_\odot = 0.28 \pm 0.08 \text{ GeV cm}^{-3}$, and we employ the exact likelihood from that analysis. This local density is consistent with several other determinations [28].

Another recent determination of the local stellar and dark matter density by McKee et al. [29] from star counts finds a significantly lower total stellar mass density than the dynamical stellar density profile measures of Refs. [27, 30, 31]. When the lower stellar density is combined with determinations of local total mass densities, McKee et al. find a higher local dark matter density $\rho_\odot = 0.49 \pm 0.13 \text{ GeV cm}^{-3}$. The error in McKee et al. of $\sigma(\rho_\odot) = 0.13 \text{ GeV cm}^{-3}$ is determined through the variation in total mass density determinations and is not from a full error analysis. Therefore, both the error and central value on the density from star counts are approximate. McKee et al. [29] also state that the dynamical estimates of the local density like that in Refs [27, 30, 31] are the “cleanest determinations of the local dark matter density,” which indicates that perhaps the current most robust determination of the local dark matter density to be coming from Zhang et al. [27].

A third recent determination of the Milky Way halo profile and local dark matter density was done by Pato et al. [32]. Pato et al. use measures of gas kinematics from neutral hydrogen terminal velocities and thickness, carbon monoxide terminal velocities, ionized hydrogen regions, and giant molecular clouds, as well as stellar and maser kinematics. They find a larger and more constrained value of the local density than Zhang et al., at $\rho_\odot = 0.420_{-0.009}^{+0.011} \pm 0.025 \text{ GeV cm}^{-3}$, while fixing the

scale radius at 20 kpc. Pato et al. find a tighter constraint on the local dark matter density. This results from their constraints on models of the entirety of the Milky Way rotation curve, with multiple kinematic sets of data to measure the local dark matter density. Using multiple local and non-local observables to measure the local dark matter density has the capacity to over-constrain the dark matter profile and its local density, therefore underestimating the true uncertainty in the local density. Exploring the multiple constraint problem on the Milky Way's density profile from kinematic data is beyond the scope of the work here. Therefore, we adopt the local density in Ref. [32] as a third local dark matter density determination in our analysis.

Other local density determinations are consistent approximately within the range of our three density determination representative results. For example, Refs. [33, 34] find $\rho_{\odot} = 0.43_{-0.10}^{0.11} \text{ GeV cm}^{-3}$; while Ref. [35] find $\rho_{\odot} = 0.20 - 0.56 \text{ GeV cm}^{-3}$ at 1σ . Our constraint from Zhang et al. [27] represents the lower range of density determinations, while McKee et al. [29] represents the higher density determinations. The framework provided here for assessing the consistency between the GCE and dwarfs, along with the open-source software, may be adapted to any chosen density and profile determinations from past or future data.

The constraints on the Milky Way halo scale radius are derived from the concentration, defined as $c \equiv R_{vir}/R_s$. The concentration of a halo describes the scale at which the slope of the profile of the halo changes from γ to 3, and it has some scatter associated with it [36]. We adopt the halo concentration's dependence on the mass of that halo as parameterized by Sanchez-Conde & Prada [37]. The concentration is log-normally distributed with an error of 0.14 dex so the prior likelihood for the scale radius is of the form:

$$\log \mathcal{L} = -\frac{(\log_{10}(R_{vir}/R_s) - \log_{10} c(M_{vir}))^2}{2 \times 0.14^2}. \quad (3.7)$$

The concentration, which sets the scale radius, will change with varying halo mass. However, over a wide range of halo masses ($5 \times 10^{11} - 10^{14} M_{\odot}$) the concentration varies only by an amount less than the statistical variation of the concentration: 0.14 dex. Hence, we neglect the additional uncertainty associated with varying the halo mass.

There is some uncertainty whether the Milky Way follows a concentration-mass relation. Indeed, Nesti & Salucci [34] find that the Milky Way is an outlier and has a value for the concentration parameter that is larger than would be implied from Sanchez-Conde & Prada's concentration-mass relation. However, the scale radius found by Nesti & Salucci is well outside the solar radius. In this regime, uncertainty in the solar radius translates into a relatively small uncertainty in the J-factor. Ultimately, the additional uncertainty introduced by Nesti & Salucci is bracketed by the considerations already discussed.

The inner profile of the Milky Way halo within the inner $\lesssim 500$ pc relevant for the GCE is not well determined by dynamical data, or numerical results, since the region becomes baryon-density dominated. However, the profile is constrained by the observed GCE itself. In the analysis including bremsstrahlung emission, Abazajian et. al. [22] find $\gamma = 1.12 \pm 0.05$. When including the newly discovered IC component, the best-fit profile shifted to $\gamma = 1.0$ with comparable errors [4].

To demonstrate the effect of allowing the parameters of the Milky Way's dark matter halo to vary, we plot in Fig. 1 the likelihood of the J-factor derived from the relaxing the values of the local density, scale radius, and slope of the inner profile. The width of the likelihood distribution of the J-factor expands the posterior likelihood of the dark matter particle mass and cross section relative to using fixed values for the halo parameters. As Fig. 1 shows, varying the local density accounts for most of the width of the J-factor likelihood, though varying the scale radius and the inner profile slope also widens the likelihood. The J-factor likelihood is approximately a normal distribution as it is dominated by an approximately normal distribution in the ρ_{\odot} uncertainty, and sub-dominant log-normal R_s and normal γ distributions.

Because integrating the likelihoods over the nuisance subspace can be computationally expensive, we approximate this integral by maximizing the log-likelihood over that subspace. Since the likelihood functions are approximately Gaussian (ρ_{\odot} and γ) or log-normal (R_s) in the nuisance parameters, this is expected to be a good approximation. We have tested that this approximation is valid by explicitly integrating the likelihoods for single parameter dimensions. We explicitly calculate the probability contained within some $\Delta \log(\mathcal{L})$ by integrating the likelihood to find the 68%, 95%, and 99.7% and 99.99997% credible intervals for our plotted results. Note that the maximization of the probability distribution leaves our results, up to an arbitrary normalization, equivalent to the frequentist profile likelihood method of finding statistical errors on parameters of interest when nuisance parameters are involved.

We determine the uncertainty regions of the particle mass and cross section parameter space for both b -quark and τ -lepton annihilation channels, as shown in Fig. 2. In the next section, we investigate the systematic uncertainty associated with uncertainties in the background-dominated low energy data portion of the GCE, as well as uncertainties introduced by incorporating or excluding different background diffuse emission models, including the bremsstrahlung excess and IC component.

IV. BACKGROUND DIFFUSE EMISSION MODEL DEPENDENCE

We test the model dependence associated with emission from astrophysical backgrounds, including the detected bremsstrahlung diffuse excess component and IC

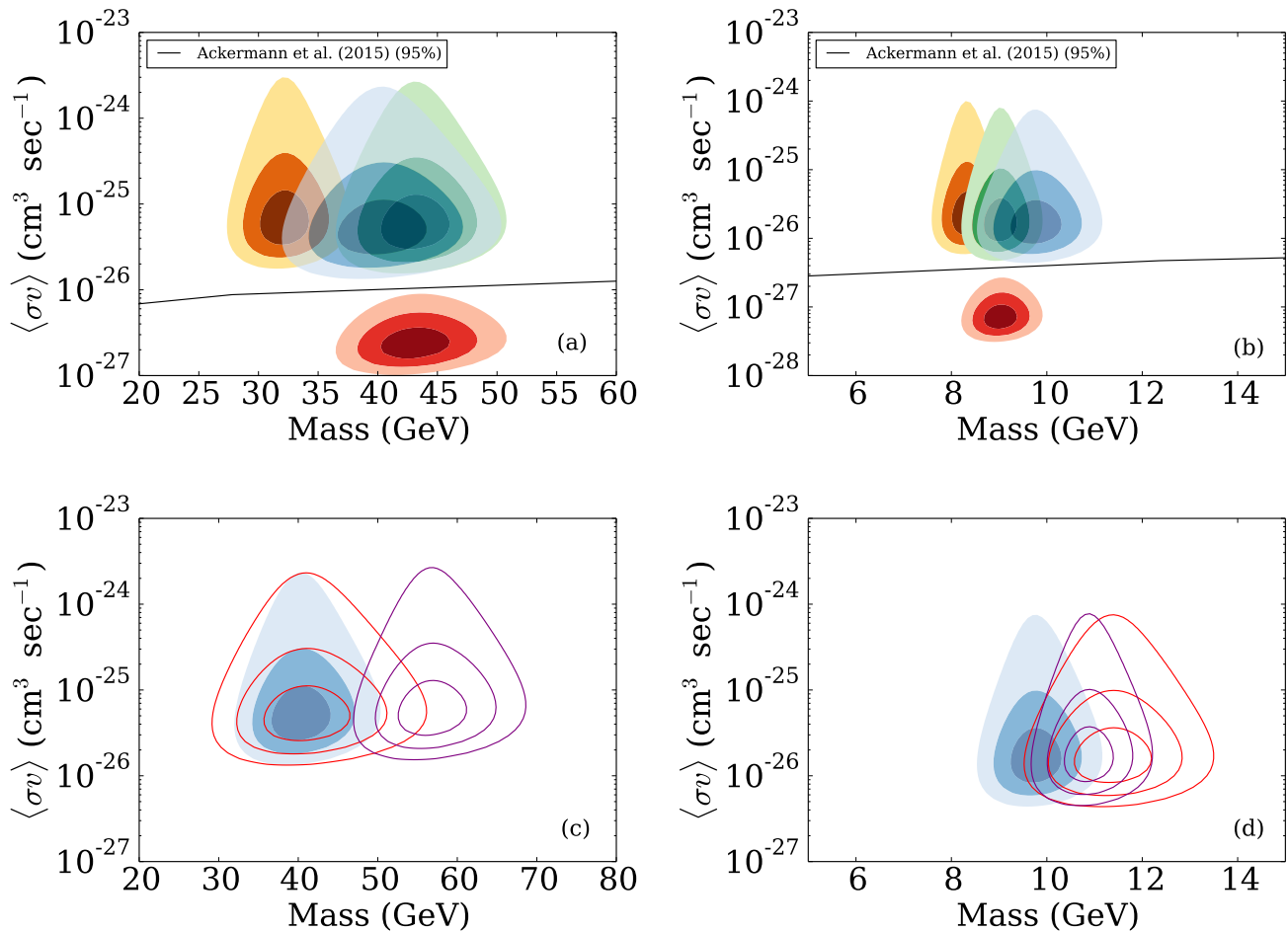


FIG. 2. In (a) & (b), we plot contours of the $\Delta\log$ -likelihood that correspond to 68%, 95% and 99.7% credible regions for the full IC, noIC, and noB data sets, when marginalizing over Milky Way halo uncertainties, which demonstrate the systematic errors involved in the inclusion of diffuse sources in the GC; (a) is for the b/\bar{b} -quark channel and (b) is for the τ^\pm channel. The full IC model is shown in blue, noIC is in orange, and noB is in green. We also show, in red contours, a non-standard high-concentration/contraction Milky Way halo model that would escape dwarf galaxy limits, but would be in conflict with local density and Milky Way halo simulations. We also show the 95% limits from dwarf galaxy searches by Ackermann et al. [19]. In the (c) & (d), for the b/\bar{b} -quark and τ^\pm channels respectively, we plot contours of the $\Delta\log$ -likelihood that correspond to 68%, 95% and 99.7% for different numbers of low-energy bins excluded, demonstrating GCE spectrum determination systematic uncertainties in our method. The red contours are those derived from excluding data below 2.03 GeV, blue from excluding data below 1.24 GeV, and purple with a 0.764 GeV cut. The blue contours are for our optimal GCE spectrum determination, as described in the text.

components producing gamma-ray emission within the GC. Since the morphology of these sources is not known a priori, there is a significant systematic uncertainty introduced by the templates adopted as the model of these diffuse sources. To bracket this model uncertainty, we take extreme cases where the model components are either present or not. Our full model in this work includes all components: the 20 cm bremsstrahlung, IC, and GCE templates, as well as new diffuse and point sources as described in Abazajian et al. [4]. The noIC (denoted ‘full’ in Abazajian et al. [22]) model includes everything from the full model except the IC component. The noB model neglects the contribution from the 20 cm template, in ad-

dition to neglecting the IC component. Including different gamma-ray source templates shifts the best-fit values of the mass, bracketing a large part of the model dependence of the GCE emission, as shown in the upper panels of Fig. 2. The dependence largely in particle mass in our diffusion uncertainties and not annihilation rate comes from the well-determined nature of the GCE total flux at ≈ 3 GeV even for various diffuse model and GCE spectral cases, as shown in Fig. 4 and Fig. 10 of Ref. [22]. Our adopted full model fit is shown in solid colors, with the contours representing an estimate of background uncertainties.

Additional systematic effects are associated with the

low-energy data points. The full low-energy data in the GCE are generally not sensitive to variations in the assumed dark matter spectra since dark matter is sub-dominant to the background components at low energies (< 1 GeV); see, e.g., Fig. 6 of Ref. [22]. Since we are not performing a full template and point source fit in this analysis, we approximate the sub-dominant nature of these low-energy data points by excluding those that are below the flux of other diffuse sources from our fits. In full template fits of Refs. [4, 22], the sub-dominant flux of the GCE portion of the template at low energies does not contribute significantly to the total fit likelihood. Including all of these points biases the best-fit masses since the GCE errors at low energy underestimate the full model error, and shift the best-fit dark matter particle mass determinations relative to the full template analysis from the same data in the full template and point source analyses. We investigate the bias effect by varying the number of low-energy data points included in the analysis. We iteratively exclude points below 0.764 GeV, 1.24 GeV, or 2.03 GeV. Variation of the low-energy data point inclusion shifts the best-fit mass by approximately 10 GeV for the b -quark annihilation channel, and by around 2 GeV for the τ -lepton annihilation channel, as shown in the lower panels of Fig. 2. Including all the lower energy data shifts to higher particle mass for the fit. Our best estimate of the subset that represents the full template and point source analysis is where the data simultaneously dominates above the background sources at $\gtrsim 1$ GeV, becomes less sensitive to the number of points included, and provides optimal sensitivity to the particle mass, as shown in Fig. 2. The optimal case is shown in solid colors.

Given that the parameter space for the GCE signal may be significantly constrained by searches for annihilation in dwarf galaxies, particularly in the Pass 8 analysis of Ref. [19], we explore the type of alteration of the Milky Way halo marginally consistent with dynamical measures and allowing for a significantly larger integrated J-factor toward the center of the galaxy: first, we take the local density to be $\rho_{\odot} = 0.4$ GeV cm $^{-3}$, which is 1.5σ away from the constraints from Zhang et al. [27]; and second, we adopt the concentration to be a highly non-standard $c = 50$, which forces the scale radius of the Milky Way to be within the R_{\odot} , boosting the inner galaxy density. Increasing the concentration approximates a new scale possible in the dark matter halo from baryonic effects.

NFW halos are potentially modified by the presence of baryons via adiabatic “contraction” of the halos. Therefore, we also explore this enhancement with the CONTRA tool provided by Ref. [38]. Qualitatively, the contracted profiles give a new effective scale radius close to R_{\odot} , and a significant enhancement of density within R_{\odot} , up to factors of ~ 1.5 . This boosts the J-factor by ~ 6 , with a commensurate reduction in the necessary $\langle\sigma v\rangle$ by that amount. Therefore, the non-standard high-concentration NFW case we propose could be plausible in some cases of contracted profiles. Though the NFW

parameters in a pure NFW sense are extreme, the overall J-factor result is within the realm of possibility in contracted profiles. A full scan of halo contraction involves an analysis that exceeds the current tools like CONTRA, and is beyond the current scope of the paper. The “high-concentration/contraction” case shown in Fig. 2 is plausible when considering particle physics models that directly escape the dwarf galaxy bounds.

V. DISCUSSION AND CONCLUSIONS

We show the credible intervals or regions consistent with three different determinations of the local density convolved with the full Milky Way halo profile uncertainties in Fig. 3, and two of the three local density determinations’ parameter regions are in significant tension with the dwarf galaxy constraints. Our results show that allowing the local density to vary increases the errors greatly along the cross section axis, leaving the mass axis less constrained. This is because the effects of cross section and the J-factor—and by extension the local density, scale radius, and inner profile slope—are exactly inversely degenerate when fitting the data. In particular, the inverse correlation between dark matter density and $\langle\sigma v\rangle$ extends the error region asymmetrically upward. This is contrast to a symmetric error in log-space, which would extend asymmetrically downward. This illustrates the importance of a full error analysis in quantifying uncertainties.

We also examine the background model dependence and low-energy intensity uncertainty, which shifts the particle mass in a systematic fashion, at the level of up to 10 GeV, depending on the overall level of these systematic uncertainties. We calculate the best fit dark matter particle mass and interaction cross section implied by the GCE that takes into account the uncertainties in the Milky Way’s halo parameters and background model uncertainties. When adopting the SDSS K-dwarf Zhang et al. [27] density estimate models for the Milky Way halo and background diffuse emission models, we found for the b -quark annihilation channel that

$$m_{\chi} = 43. \left(\begin{smallmatrix} +2.1 \\ -1.9 \end{smallmatrix} \text{ stat.} \right) (\pm 19. \text{ sys.}) \text{ GeV}, \quad (5.1)$$

$$\langle\sigma v\rangle_{bb} = 7.4 \left(\begin{smallmatrix} +2.7 \\ -2.3 \end{smallmatrix} \right) \times 10^{-26} \text{ cm}^3 \text{ s}^{-1}. \quad (5.2)$$

For the τ -lepton channel, we found

$$m_{\chi} = 9.0 \left(\begin{smallmatrix} +0.27 \\ -0.23 \end{smallmatrix} \text{ stat.} \right) (\pm 2. \text{ sys.}) \text{ GeV}, \quad (5.3)$$

$$\langle\sigma v\rangle_{\tau} = 2.2 \left(\begin{smallmatrix} +1.2 \\ -0.7 \end{smallmatrix} \right) \times 10^{-26} \text{ cm}^3 \text{ s}^{-1}. \quad (5.4)$$

The systematic errors are defined largely by the background diffuse emission model uncertainties, which impacts the determined dark matter particle mass much more greatly than its cross section. This parameter space is significantly constrained by dwarf galaxy annihilation searches, as shown in Fig. 3. The parameter space agrees largely with other analyses. The region found by Calore et al. [12] is a bit lower due to two factors: they adopt

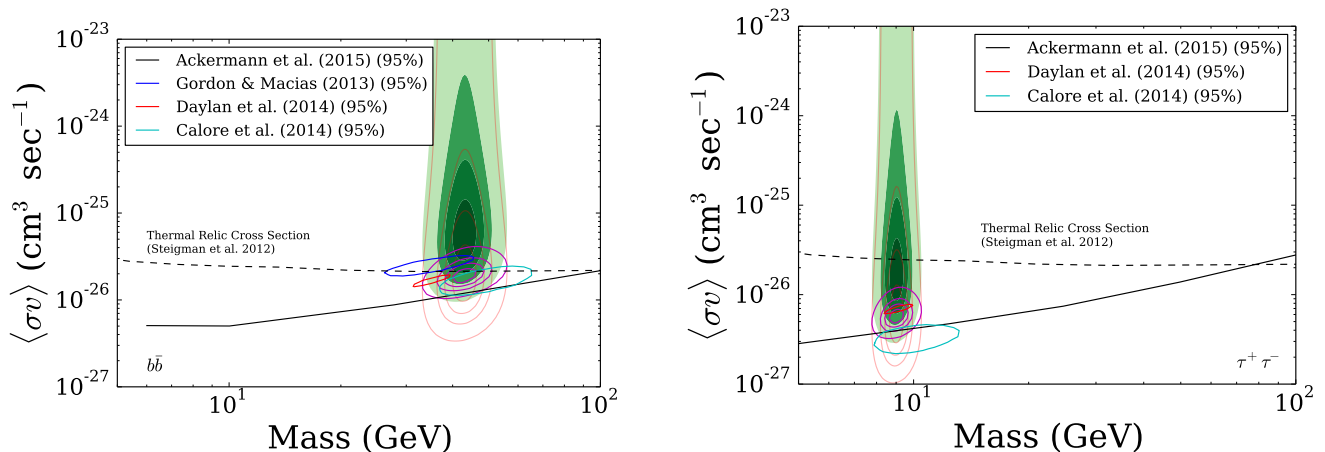


FIG. 3. Plotted in filled green are contours the $\Delta\log$ -likelihood that correspond to 68%, 95%, and 99.7% and 99.99997% credible regions (corresponding approximately to 1, 2, 3 and 5 σ) when marginalizing over Milky Way halo uncertainties, in our best estimates for background uncertainties, with the local dark matter density determination by Zhang et al. [27]. Counter to the expectation that a symmetric error becomes asymmetric in a logarithmic plot, with larger extent downward, the error regions are asymmetrically oriented upward due to the anti-correlation of the J-factor with the annihilation rate $\langle\sigma v\rangle$. We also show, in light red, the respective approximate error contours from the inferred approximate dark matter density in the low stellar density star count measures of McKee et al. [29]. In purple, we show the error contours derived from the local dark matter density of Pato et al. [32]. We also show the 95% limits from the dwarf galaxy annihilation search by Ackermann et al. [19], and the signal regions as presented in Refs. [10, 12, 13]. As seen here, both the Zhang et al. and Pato et al. local dark matter density determinations leave single-channel dark matter annihilation interpretations of the GCE in strong tension with dwarf limits. The b -quark annihilation channel is on the left and the τ -lepton annihilation channel is on the right.

a high value for $\rho_\odot = 0.4 \text{ GeV cm}^{-3}$, as well as a more peaked central profile for their fit at $\gamma = 1.2$. A more strongly peaked central profile γ allows the inner and central Galaxy dark matter density to rise to higher values, which commensurately lowers the required annihilation rate. These modifications are along the lines of Milky Way profile changes that would be required to escape dwarf constraints, as discussed above. The interaction rates for the GCE signal at these particle masses are also being tested with collider searches for specific couplings. For example, in the ATLAS searches for WIMP particle production through quark couplings via vector and axial-vector operators to dark matter constrain this region [39].

There are models for generation of the GCE from secondary emission of annihilation products that could alleviate these constraints. One such model produces the GCE as an IC emission from leptonic final states, matching the profile and spectrum but with a significantly reduced annihilation cross section [40–42]. The IC-induced GCE is generated in the high value of the GC’s interstellar radiation field, while the radiation density in dwarf galaxies is much lower, potentially allowing evasion of this tension.

Perhaps the largest systematic or modeling uncertainty is the extrapolation of the Milky Way profile from the local density determination, ρ_\odot , at R_\odot to where the GCE is bright at $\lesssim 500 \text{ pc}$, which is determined by the profile extrapolation γ . For example, a strong adiabatic contrac-

tion of the Milky Way’s dark matter halo due to baryonic infall could greatly enhance the inner Galaxy dark matter density. To illustrate a highly non-standard, yet potentially physically viable, high-concentration/contraction case that would be necessary to eliminate the constraints from dwarf galaxies, we chose a high local density and small Milky Way halo scale radius, corresponding to a high concentration or contracted profile radius, reducing the particle dark matter annihilation rate necessary for the GCE considerably and avoiding the dwarf galaxy bounds. These choices for a pure NFW halo are inconsistent with dark matter only simulations, but consistent with halo profiles that have a contracted scale radius close to R_\odot [4, 38]. However, recent dynamical plus microlensing data are inconsistent with a strongly contracted halo [43]. In addition, contraction is not seen in high-mass halo systems where it is expected to more greatly contribute [44]. Any contraction of the halo must also preserve both the local density constraints from Zhang et al. [27] and the inner halo profile required by the gamma-ray data, $\gamma = 1.0 - 1.2$. In summary, our high-concentration/contraction case appears disfavored by dynamical constraints, but evades dwarf galaxy limits and is a plausible model for exploration of particle dark matter properties. Therefore, the non-standard high-concentration NFW case we propose could resolve the tension in the case that highly contracted dark matter profiles are found for the Milky Way.

A recent study aiming to determine the local stellar

density from star counts, McKee et al. [29], has found lower stellar densities than previous analyses, such as Zhang et al. [27], Bovy & Tremaine [30], and Bovy & Rix [31], that determine the modeled stellar density profile simultaneously as the dark matter profile, using the position and velocity data of stars above the plane. If these lower stellar densities are borne out to be accurate, with the total density remaining invariant, then the dark matter density would be commensurately determined to be higher. The error analysis on the local dark matter density in McKee et al. [29] uses the variation in total mass density determinations to set the value of $\sigma(\rho_{\odot})$ and is not the result of a full error analysis. Therefore, both the error and central value on the density from star counts are approximate.

McKee et al. state that high-above the Galactic plane estimates of the local density like that in Refs [27, 30, 31] are “the cleanest determination of the local density of dark matter,” which indicates the most robust determination of the local dark matter density may be that from Zhang et al. [27]. However, if there is a systematic uncertainty that shifts local stellar densities lower, our framework and open source tools allow for a reassessment of the GCE and dwarf agreement or tension for arbitrary spectra of dark matter interpretations with any new observational constraints on Milky Way halo properties.

Another determination of the local dark matter density using a broad set of Milky Way dynamical data was found in Pato et al. [32]. In Fig. 3 we show GCE contours from the higher value of the approximate local dark matter density inferred by McKee et al. [29] in light red, and that from Pato et al. [32] in purple. Importantly, both the Zhang et al. and Pato et al. local density determinations are inconsistent with dwarf galaxy constraints at the approximately $\sim 5\sigma$ level, as shown in Fig. 3. Significantly, it has been shown in some work that the uncertainties in the dwarf galaxy dark matter profiles have been underestimated, which would alleviate their constraints and potentially relieve the GCE-dwarf tension as well [45].

In summary, we performed a Bayesian analysis of the GCE emission that more accurately accounts for uncertainties in the Milky Way halo parameters and approximates diffuse background emission model uncertainties. The presence of the GCE is relatively robust to variations

in the background models, though the best fit values of the dark matter particle mass depends significantly on these background models. Our analysis is certainly not an exhaustive search of all Milky Way halo and diffuse gamma-ray emission model uncertainties, but demonstrates the fact that uncertainties in the halo parameters increase the uncertainty in dark matter particle parameters. Significantly, however, we find that robust determinations of the Milky Way halo properties, with two key determinations of the local dark matter density [27, 32], leave the GCE parameter space in significant tension with dwarf galaxy constraints. If the local stellar density is much higher, as in Ref. [29], or the Milky Way halo’s dark matter density is significantly contracted, then the tension is relaxed. In order to make a quantitative statement as to the level of exclusion of the GCE by the combined dwarf analyses, a joint likelihood analysis of the combined dwarf and GCE constraints would need to be performed.

Though the triple consistency of the dark matter interpretation of the GCE with morphology, signal strength, and spectra remains intriguing, the tension with dwarf galaxy annihilation searches illustrated here, coupled with the changes to the Milky Way halo properties that would be needed to alleviate these constraints, may indicate that astrophysical interpretations of the GCE or more novel dark matter annihilation mechanisms are more plausible explanations of the GCE that are able to avoid constraints from dwarf galaxies. Further multiwavelength analysis is required to model background sources of gamma-rays, which constrains the associated systematics and allows insight into the true nature of the gamma-ray excess in the Galactic Center.

ACKNOWLEDGMENTS

We thank Keith Bechtol, Mike Boylan-Kolchin, James Bullock, Sheldon Campbell, Alex Geringer-Sameth, Manoj Kaplinghat, Anna Kwa and Flip Tanedo for useful discussions and comments on a draft. K.N.A. and R.K. are partially supported by NSF CAREER Grant No. PHY-11-59224 and NSF Grant No. PHY-1316792.

-
- [1] J. L. Feng, *Ann.Rev.Astron.Astrophys.* **48**, 495 (2010), arXiv:1003.0904 [astro-ph.CO].
 - [2] M. Chernyakova, D. Malyshev, F. Aharonian, R. Crocker, and D. Jones, *Astrophys.J.* **726**, 60 (2011), arXiv:1009.2630 [astro-ph.HE].
 - [3] F. Yusef-Zadeh, J. Hewitt, M. Wardle, V. Tatischeff, D. Roberts, *et al.*, *Astrophys.J.* **762**, 33 (2013), arXiv:1206.6882 [astro-ph.HE].
 - [4] K. N. Abazajian, N. Canac, S. Horiuchi, M. Kaplinghat, and A. Kwa, *JCAP* **1507**, 013 (2015), arXiv:1410.6168 [astro-ph.HE].
 - [5] L. Goodenough and D. Hooper, (2009), arXiv:0910.2998 [hep-ph].
 - [6] D. Hooper and L. Goodenough, *Phys.Lett.* **B697**, 412 (2011), arXiv:1010.2752 [hep-ph].
 - [7] D. Hooper and T. Linden, *Phys.Rev.* **D84**, 123005 (2011), arXiv:1110.0006 [astro-ph.HE].
 - [8] A. Boyarsky, D. Malyshev, and O. Ruchayskiy, *Phys.Lett.* **B705**, 165 (2011), arXiv:1012.5839 [hep-ph].
 - [9] K. N. Abazajian and M. Kaplinghat, *Phys.Rev.* **D86**, 083511 (2012), arXiv:1207.6047 [astro-ph.HE].

- [10] C. Gordon and O. Macias, *Phys.Rev.* **D88**, 083521 (2013), arXiv:1306.5725 [astro-ph.HE].
- [11] O. Macias and C. Gordon, *Phys. Rev.* **D89**, 063515 (2014), arXiv:1312.6671 [astro-ph.HE].
- [12] F. Calore, I. Cholis, and C. Weniger, *JCAP* **1503**, 038 (2015), arXiv:1409.0042 [astro-ph.CO].
- [13] T. Daylan, D. P. Finkbeiner, D. Hooper, T. Linden, S. K. N. Portillo, *et al.*, (2014), arXiv:1402.6703 [astro-ph.HE].
- [14] E. A. Baltz, J. E. Taylor, and L. L. Wai, *Astrophys. J.* **659**, L125 (2007), arXiv:astro-ph/0610731 [astro-ph].
- [15] K. N. Abazajian, *JCAP* **1103**, 010 (2011), arXiv:1011.4275 [astro-ph.HE].
- [16] R. Bartels, S. Krishnamurthy, and C. Weniger, (2015), arXiv:1506.05104 [astro-ph.HE].
- [17] S. K. Lee, M. Lisanti, B. R. Safdi, T. R. Slatyer, and W. Xue, (2015), arXiv:1506.05124 [astro-ph.HE].
- [18] A. Geringer-Sameth, S. M. Koushiappas, and M. G. Walker, *Phys. Rev.* **D91**, 083535 (2015), arXiv:1410.2242 [astro-ph.CO].
- [19] M. Ackermann *et al.* (Fermi-LAT), (2015), arXiv:1503.02641 [astro-ph.HE].
- [20] A. Geringer-Sameth, M. G. Walker, S. M. Koushiappas, S. E. Kopusov, V. Belokurov, G. Torrealba, and N. W. Evans, *Phys. Rev. Lett.* **115**, 081101 (2015), arXiv:1503.02320 [astro-ph.HE].
- [21] P. L. Nolan, A. A. Abdo, M. Ackermann, M. Ajello, A. Allafort, E. Antolini, W. B. Atwood, M. Axelsson, L. Baldini, J. Ballet, and *et al.* (Fermi-LAT Collaboration), *Astrophys.J.Suppl.* **199**, 31 (2012), arXiv:1108.1435 [astro-ph.HE].
- [22] K. N. Abazajian, N. Canac, S. Horiuchi, and M. Kaplinghat, *Phys.Rev.* **D90**, 023526 (2014), arXiv:1402.4090 [astro-ph.HE].
- [23] E. L. Wright *et al.*, *Astron. J.* **140**, 1868 (2010), arXiv:1008.0031 [astro-ph.IM].
- [24] J. F. Navarro, C. S. Frenk, and S. D. M. White, *Astrophys. J.* **490**, 493 (1997), arXiv:astro-ph/9611107.
- [25] A. Klypin, H. Zhao, and R. S. Somerville, *Astrophys. J.* **573**, 597 (2002), arXiv:astro-ph/0110390.
- [26] M. Cirelli, G. Corcella, A. Hektor, G. Hutsi, M. Kadastik, *et al.*, *JCAP* **1103**, 051 (2011), arXiv:1012.4515 [hep-ph].
- [27] L. Zhang, H.-W. Rix, G. van de Ven, J. Bovy, C. Liu, and G. Zhao, *Astrophys. J.* **772**, 108 (2013), arXiv:1209.0256 [astro-ph.GA].
- [28] J. I. Read, *J. Phys.* **G41**, 063101 (2014), arXiv:1404.1938 [astro-ph.GA].
- [29] C. F. McKee, A. Parravano, and D. J. Hollenbach, *Astrophys. J.* **814**, 13 (2015), arXiv:1509.05334 [astro-ph.GA].
- [30] J. Bovy and S. Tremaine, *Astrophys.J.* **756**, 89 (2012), arXiv:1205.4033 [astro-ph.GA].
- [31] J. Bovy and H.-W. Rix, *Astrophys. J.* **779**, 115 (2013), arXiv:1309.0809 [astro-ph.GA].
- [32] M. Pato, F. Iocco, and G. Bertone, *JCAP* **1512**, 001 (2015), arXiv:1504.06324 [astro-ph.GA].
- [33] P. Salucci, F. Nesti, G. Gentile, and C. F. Martins, *Astron. Astrophys.* **523**, A83 (2010), arXiv:1003.3101 [astro-ph.GA].
- [34] F. Nesti and P. Salucci, *JCAP* **1307**, 016 (2013), arXiv:1304.5127 [astro-ph.GA].
- [35] F. Iocco, M. Pato, G. Bertone, and P. Jetzer, *JCAP* **1111**, 029 (2011), arXiv:1107.5810 [astro-ph.GA].
- [36] J. S. Bullock, T. S. Kolatt, Y. Sigad, R. S. Somerville, A. V. Kravtsov, A. A. Klypin, J. R. Primack, and A. Dekel, *Mon. Not. Roy. Astron. Soc.* **321**, 559 (2001), arXiv:astro-ph/9908159 [astro-ph].
- [37] M. A. Sanchez-Conde and F. Prada, *Mon. Not. Roy. Astron. Soc.* **442**, 2271 (2014), arXiv:1312.1729 [astro-ph.CO].
- [38] O. Y. Gnedin, D. Ceverino, N. Y. Gnedin, A. A. Klypin, A. V. Kravtsov, R. Levine, D. Nagai, and G. Yepes, *ArXiv e-prints* (2011), arXiv:1108.5736 [astro-ph.CO].
- [39] G. Aad *et al.* (ATLAS), *JHEP* **04**, 075 (2013), arXiv:1210.4491 [hep-ex].
- [40] M. Kaplinghat, T. Linden, and H.-B. Yu, *Phys. Rev. Lett.* **114**, 211303 (2015), arXiv:1501.03507 [hep-ph].
- [41] F. Calore, I. Cholis, C. McCabe, and C. Weniger, *Phys. Rev.* **D91**, 063003 (2015), arXiv:1411.4647 [hep-ph].
- [42] J. Liu, N. Weiner, and W. Xue, *JHEP* **08**, 050 (2015), arXiv:1412.1485 [hep-ph].
- [43] J. Binney and T. Piffl, (2015), *Mon. Not. Roy. Astron. Soc.* accepted, arXiv:1509.06877 [astro-ph.GA].
- [44] A. B. Newman, T. Treu, R. S. Ellis, D. J. Sand, C. Nipoti, J. Richard, and E. Jullo, *Astrophys. J.* **765**, 24 (2013), arXiv:1209.1391 [astro-ph.CO].
- [45] V. Bonnivard, C. Combet, D. Maurin, and M. G. Walker, *Mon. Not. Roy. Astron. Soc.* **446**, 3002 (2015), arXiv:1407.7822 [astro-ph.HE].